Journal of Structural Geology 33 (2011) 154–168

Contents lists available at ScienceDirect

Journal of Structural Geology

journal homepage: www.elsevier.com/locate/jsg

Pressure solution-fracturing interactions in weakly cohesive carbonate sediments and rocks: Example of the synsedimentary deformation of the Campanian chalk from the Mons Basin (Belgium)

J. Richard*, J.P. Sizun

U.M.R. C.N.R.S. 6249 Chrono-environnement, Département de Géosciences, U.F.R. Sciences et Techniques, Université de Franche-Comté, 16 route de Gray, 25030 Besançon cedex, France

ARTICLE INFO

Article history:
Received 23 June 2010
Received in revised form
4 November 2010
Accepted 17 November 2010
Available online 27 November 2010

Keywords:
Deformation
Pressure solution
Mass transfer
Fracture
Diagenesis
Carbonate

ABSTRACT

This paper documents the pressure solution-fracturing interactions in weakly cohesive carbonate sediments and rocks by studying the synsedimentary deformation of the Campanian chalk from the Mons Basin (Belgium). The present work shows that the development of a normal fault in a near-surface marine environment can promote significant mass transfers and volume changes in weakly cohesive micritic carbonate materials. The deformation corresponds to a mass redistribution from the deformed zones adjacent to the fault plane towards the outermost deformed zones. These mass transfers result from a faster return of the interstitial fluid pressure to an initial state within the outermost deformed zones. The deformation is rapidly controlled by the volume gains caused by the diffused rupture of grain contacts inside the outermost deformed zones and not by fracturing. Within the deformed zones adjacent to the fault plane, the mass losses and the related chemical compaction lead to a decrease in reservoir qualities of the material and the growth of a permeability barrier that rapidly restricts the flow of interstitial fluids towards the active fractures. Within the outermost deformed zones, the transport properties and the reservoir qualities of the material are maintained or increased.

1. Introduction

Pressure solution (fluid-enhanced deformation) is considered to be a major mechanism of rock deformation. In the upper crust, it often plays an important role within zones where it is spatially associated with brittle deformation (Gratier et al., 1999). Previous contributions (Mimran, 1975, 1977; Jones et al., 1984; Carrio-Schaffhauser and Gaviglio, 1990; Hellmann et al., 2002a, b; Angelier et al., 2006; Schroeder et al., 2006; Darquennes et al., 2007; Richard et al., 2002; Richard, 2008; Gaviglio et al., 1993, 1997, 1999, 2009) highlighted the interest to study the interactions between pressure solution and fracturing by examining the experimental and natural deformation in carbonate rocks and particularly in chalk. A small number of these works focussed on the mass transfers and volume changes caused by the pressure solution-fracturing interactions and attempted to make clear, at the grain scale, the diagenetic processes at the origin of these mass transfers and volume changes. A first study (Richard, 2008) highlighted the interest of this approach to develop physico-chemical models of deformation mechanisms. The present paper completes this first study by examining the synsedimentary deformation of the Campanian chalk from the Mons Basin in a near-surface marine environment.

Several works (Angelier et al., 2006; Schroeder et al., 2006; Darquennes et al., 2007; Gaviglio et al., 1993, 1997, 1999, 2009) were devoted to the study of interactions between pressure solution and fracturing processes in chalk from the Mons Basin. These previous contributions have chiefly provided data about the petrophysical and petrographic impact of the pressure solution-fracturing interactions but did not examine the mass and volume changes caused by these mechano-chemical interactions. Moreover, the modifications of transport properties of chalk (essential for petroleum geologists) were poorly documented and no physico-chemical model of the deformation mechanism was proposed. The purpose of the present paper is therefore (1) to qualitatively and quantitatively characterise the diagenetic signature (modifications of reservoir qualities and transport properties, elemental signature and nannofacies of chalk) of pressure solution-fracturing interactions caused by the development of a dip-slip normal fault in the "white chalk" from the Mons Basin, (2) to quantify the mass transfers and volume changes, to determinate their spatial distribution

* Corresponding author. Tel.: +33 3 81666434; fax: +33 3 81666558.
E-mail address: james.richard@univ-fcomte.fr (J. Richard).

0191-8141/$ – see front matter © 2010 Elsevier Ltd. All rights reserved.
doi:10.1016/j.jsg.2010.11.006

and to make clear, at the grain scale, the diagenetic processes at the origin of these mass and volume changes and (3) to propose a physico-chemical model of the deformation mechanism.

2. Geological setting

The Mons Basin (30 km long and 15 km wide) that constitutes a northern extension of the Paris Basin is located in southwestern Belgium (Fig. 1). It is filled by Cretaceous and Cenozoic deposits that unconformably overlap the Paleozoic basement (Fig. 1).

Detailed tectonic investigations have been carried out in the Mons Basin (Vandycke et al., 1988, 1991; Vandycke and Bergerat, 1989; Vandycke, 2002). They highlighted that the Late Cretaceous tectonics was dominated by an extensional regime (NW–SE extension during the Late Campanian followed by a NE–SW extension during the Maastrichtian) interrupted by a strike-slip event during the Early Maastrichtian. The Late Campanian NW–SE extension led to the development of N040°E to N055°E normal faults, often associated with subvertical joints. The field observations indicate that normal faulting related to the Late Campanian

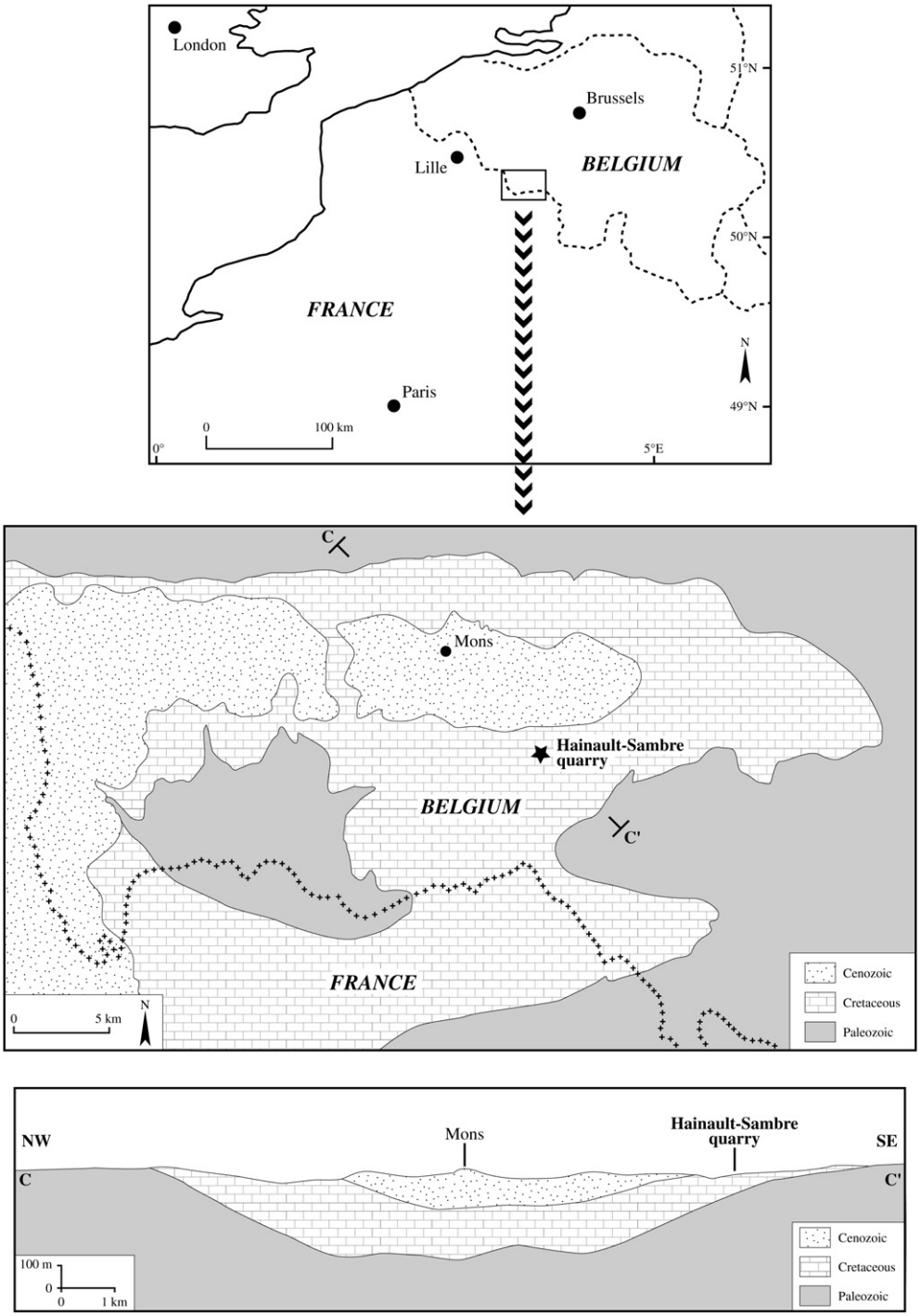

Fig. 1. Geological map and geological section of the Mons Basin with location of the Hainault–Sambre quarry.

NW–SE extension results from a synsedimentary tectonics that probably played an important role in the basin subsidence (Vandycke et al., 1991).

3. Sampling, analytical techniques and methods

3.1. Sampling

Core samples were collected in the Hainault–Sambre quarry located in the southern part of the Mons Basin near Harmignies (Fig. 1). The studied fault system results from the development of a dip-slip normal fault through a "white chalk" (insoluble residue below 3%) in the Obourg Chalk (Late Campanian lithostratigraphic unit). It shows a principal fault plane with subsidiary branches (Fig. 2). The strike of the principal fault plane F is N055°E, its dip is 67°S and the throw reaches 1.7 m (Fig. 2). The strike of the principal fault plane indicates that the studied fault system is related to the Late Campanian NW–SE extension and consequently to synsedimentary tectonics.

Two cores (7 cm in diameter) were drilled at right angles with the strike of the principal fault plane in a horizontal position (at the core scale, the bedding plane can be considered as horizontal): one of 58.6 cm long through the hangingwall and one of 76.9 cm long through the footwall (Fig. 2). Both were drilled 1.2 m below a key

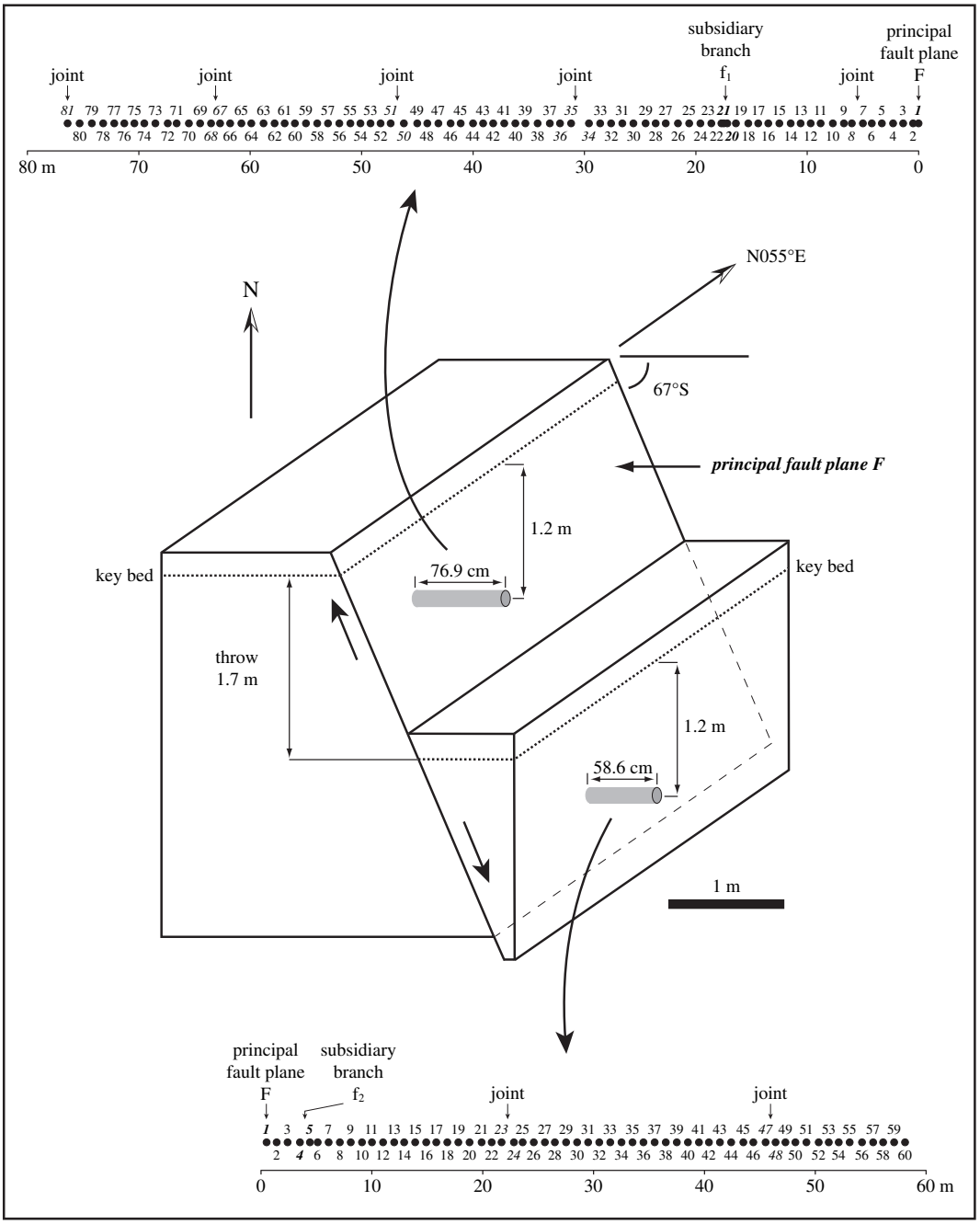

Fig. 2. Simplified sketch of the studied working face with location of samples. The studied fault system shows a principal fault plane (F) with subsidiary branches. The strike of the principal fault plane is N055°E, its dip is 67°S and the throw reaches 1.7 m. Two cores were drilled at right angles with the strike of the principal fault plane in a horizontal position: one of 58.6 cm long through the hangingwall and one of 76.9 cm long through the footwall. Both were drilled 1.2 m below a key bed with belemnites. They crosscut the principal fault plane (F), two of its subsidiary branches (f_1 and f_2) and joints. The samples showing a fault plane are in bold and italic whereas the samples showing a joint are in italic.

bed with belemnites (Fig. 2). They crosscut the principal fault plane F, two of its subsidiary branches (f_1 and f_2) and several joints (Fig. 2).

3.2. Analytical techniques

3.2.1. Geochemical analyses

The concentrations of 53 elements were measured in S.A.R.M. (Service d'Analyse des Roches et des Minéraux, Vandoeuvre-lès-Nancy, France) by:

- ICP-AES: Al, Ca, Fe, K, Mg, Mn, Na, P, Si, Ti;
- ICP-MS: As, Ba, Be, Bi, Cd, Ce, Co, Cr, Cs, Cu, Dy, Er, Eu, Ga, Gd, Ge, Hf, Ho, In, La, Lu, Mo, Nb, Nd, Ni, Pb, Pr, Rb, Sb, Sm, Sn, Sr, Ta, Tb, Th, Tm, U, V, W, Y, Yb, Zn and Zr;
- and AAS: Al.

The samples were ground to fine powders in an agate ball mill. Subsamples were fused with lithium metaborate and the melts dissolved in acid solutions. The concentrations are expressed in parts per million (ppm). In the concentration ranges observed in this study, the analytical accuracy is:

- <5% for Ca, Sr and Y;
- <10% for Al, Ba, Er, Eu, Hf, La, Nd, Si, V, Yb and Zn;
- <15% for Ce, Gd, Mg, Nb, Pr, Rb, Sb, Sm, Sn, Th, U and Zr;
- <20% for Ga, Co, Cr, Cs, Cu, Dy, Fe, Ho, Lu, P, Ta, Tb and Tm;
- >20% for As, Cd, Mo and Pb.

3.2.2. Pore space characterisation

Water porosimetry measurements were performed to determine the bulk density and the total porosity. The samples were dried at 60 °C until they reached a stable mass (M_d). They were then degassed during 24 h in an air-tight enclosure before being progressively saturated, from their bottom, with a degassed and distilled water under a dynamic vacuum. The bulk density (ρ) and the total porosity (Φ) are given by the expressions:

$$\rho = M_d/(M_1 - M_2)$$

$$\Phi = ((M_1 - M_d)/(M_1 - M_2)) \times 100$$

where M_1 is the mass of the sample entirely saturated with a degassed and distilled water and M_2 is the mass of the underwater sample (hydrostatic weight). The analytical accuracies are ± 0.002 (ρ) and ±0.05% (Φ).

Measurements by mercury injection porosimetry were made by using a Micromeritics PoreSizer Autopore IV porosimeter. They allowed to clarify the distribution of pore access radii between 200 and 0.003 μm, to quantify the trapped porosity and to determine the threshold radii. The trapped porosity percentage (Φ_t) is given by the expression:

$$\Phi_t = (\Phi_1/\Phi_2) \times 100$$

where Φ_1 is the porosity filled by liquid mercury at the end of the extrusion cycle and Φ_2 the porosity filled by liquid mercury at the end of the intrusion cycle. The analytical accuracy is ±0.05%. The threshold radius r_a (Dullien, 1979) was calculated from equations of secant tangents at the base of the cumulative pore volume versus pore access radius curve (first injection). The analytical accuracy ranges from ±0.001 μm ($r_a \approx 0.04$ μm) to ± 0.01 μm ($r_a \approx 2$ μm).

The gas permeability measurements were performed with a Hassler cell using nitrogen. During the measurements the flow was laminar (Reynolds number below 0.001) and the lateral pressure and the pressure gradient were equal respectively to 0.20 and 0.16 MPa. The analytical accuracy varies between ±10% ($k \approx 1$ D) and ±0.5% ($k \approx 0.001$ mD).

3.3. Mass and volume changes: method

Isocon method is an effective means of quantitatively evaluating changes in mass and volume in a wide range of geological processes (Grant, 1986, 2005). In the isocon analysis, the Gresens' equation (Gresens, 1967) was rewritten as:

$$C_i^A = M^O/M^A\left(C_i^O + \Delta C_i\right) \quad (1)$$

where C_i^O and C_i^A are the concentrations of the major or trace element i in the original and altered rock respectively, M^O and M^A are the masses of the original and altered rock respectively and ΔC_i denotes the change in concentration of the major or trace element i between the original and altered rock. For an immobile element, Eq. (1) can be written:

$$C_i^A/C_i^O = M^O/M^A = 1 \quad (2)$$

because $\Delta C_i = 0$. The masses of the original and altered rock (M^O and M^A respectively) can be expressed by the formulae:

$$M^O = \rho^O \times V^O \quad (3)$$

$$M^A = \rho^A \times V^A \quad (4)$$

where ρ is the bulk density and V the volume. Combining Eq. (2) with Eqs. (3) and (4), we can write:

$$C_i^A/C_i^O = M^O/M^A = \left(\rho^O \times V^O\right)\Big/\left(\rho^A \times V^A\right) = 1 \quad (5)$$

Eq. (5) allows to calculate the changes in volume and mass by using the analytical data C_i^O, C_i^A , ρ^O and ρ^A:

$$V^O/V^A = \left(C_i^A/C_i^O\right) \times \left(\rho^A/\rho^O\right) \quad (6)$$

$$M^O/M^A = \left(\rho^O/\rho^A\right) \times \left(V^O/V^A\right) = C_i^A/C_i^O \quad (7)$$

V^O/V^A (or M^O/M^A) > 1 indicates a volume (or mass) loss, V^O/V^A (or M^O/M^A) < 1 indicates a volume (or mass) gain, V^O/V^A (or M^O/M^A) = 1 indicates an alteration without change in volume (or mass). The volume and mass changes are given in %.

4. Results

4.1. Petrophysical signature of the deformation

4.1.1. Total porosity

The total porosity versus sample position curve reveals that the original chalk from the footwall and the hangingwall has two different signatures (Fig. 3). The footwall and the hangingwall were therefore investigated by using different reference values: 40.38–41.00% and 42.37–43.07% respectively. Considering these reference values, it appears that the total porosity is modified within a 43.3 ± 1.9 cm wide zone (Fig. 3): 19.1 ± 0.5 cm in the footwall (samples 1 to 23–24) and 24.2 ± 1.4 cm in the hangingwall (samples 1 to 24–27).

In the footwall (Fig. 3), the total porosity decreases within an internal zone (samples 1 to 9–10) and it increases within an external zone (samples 10–11 to 18–19). The lowest value (36.28%)

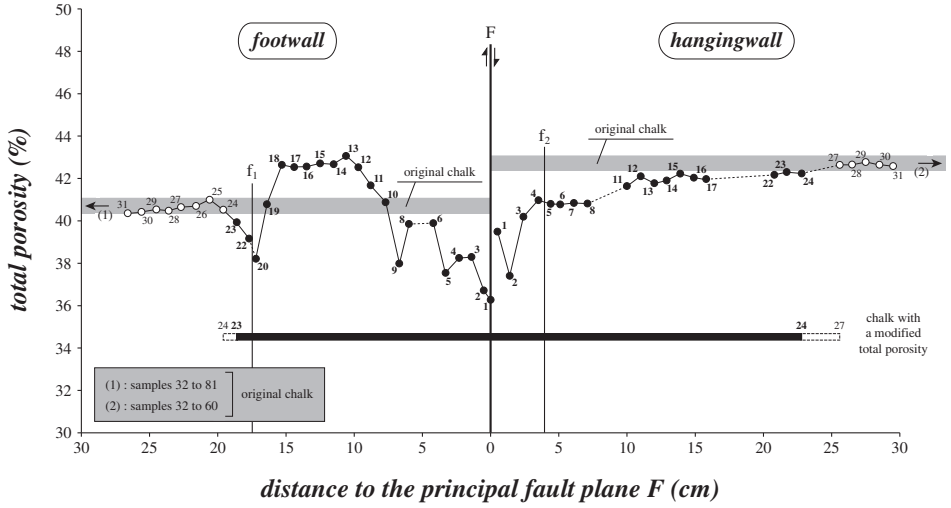

Fig. 3. Evolution of the total porosity of chalk through the footwall and the hangingwall of the studied fault system.

is observed on the principal fault plane (sample 1). A total porosity depletion is also observed on both sides of the subsidiary branch f_1 within a 2.8 ± 1.4 cm wide zone (samples 19–20 to 23–24) but this depletion is less important than the decrease linked to the principal fault plane.

In the hangingwall (Fig. 3), the total porosity decreases from 42.37 to 43.07% (original chalk) to a minimum of 37.40% (sample 2). Several differences are observed between the hangingwall and the footwall: in the hangingwall, [1] the total porosity does not increase within an external zone, [2] the lowest value (sample 2) is not observed on the principal fault plane but at 1.4 cm from it and [3] the development of the subsidiary branch f_2 did not lead to any change in total porosity.

4.1.2. Threshold radius and trapped porosity

In the footwall as well as in the hangingwall, the decrease in total porosity is correlated with a decrease in threshold radii (Fig. 4): from 0.38 μm (original chalk samples 29 and 57) to 0.34 μm (lowest value, sample 3) and from 0.43 to 0.46 μm (original chalk samples 31 and 55) to 0.35 μm (lowest value, sample 2) respectively. The lowest threshold radii (footwall sample 3, hangingwall sample 2) are not observed on the principal fault plane but at 1.4 cm from it (Fig. 4). The samples closer to the principal fault plane (footwall samples 1 and 2, hangingwall sample 1) show larger threshold radii (Fig. 4). It is notably the case of footwall sample 1 that exhibits a value higher than the original chalk values. Footwall samples 13 and 15 (Fig. 4) indicate that the increase in total porosity observed from samples 10–11 to 18–19 (Fig. 3) is correlated with an increase in threshold radius.

Significant changes in trapped porosity are only observed in the two sides of the principal fault plane between 0.5 and 1.4 cm (Fig. 4): the trapped porosity increases in the footwall and decreases in the hangingwall. On the principal fault plane (footwall sample 1), no change is observed (Fig. 4).

4.1.3. Permeability

Gas permeability measurements were performed using subcores (1 cm in diameter, between 0.8 and 2.7 cm in length) perpendicular or parallel to the principal fault plane and drilled in the bedding plane.

In the footwall as well as in the hangingwall, the permeability of perpendicular subcores varies with the distance to the principal fault plane (Fig. 5). In the two sides of the principal fault plane, a permeability depletion correlated with a decrease in total porosity is observed (Fig. 5):

- within the footwall, the permeability decreases from 3.92 mD (original chalk) to 2.41 mD (lowest value, sample A) within a 6.9 ± 2.7 cm wide zone (from samples C–B to the principal fault plane);
- within the hangingwall, the permeability decreases from 3.38 to 3.63 mD (original chalk) to 2.20 mD (lowest value, sample a) within a 4 ± 0.6 cm wide zone (from samples c–b to the principal fault plane).

In the footwall as well as in the hangingwall, the lowest values (samples A and a respectively) are observed on the principal fault plane (Fig. 5). Hangingwall sample d reveals that the low decreases in total porosity are not correlated with significant changes in permeability (Fig. 5). Footwall sample D (Fig. 5) indicates that the increase in total porosity observed within the footwall from samples 10–11 to 18–19 (Fig. 3) can be correlated to a significant increase in permeability.

The permeability of parallel subcores ranges from 2.38 to 7.41 mD. It is not correlated with the distance to the principal fault plane.

4.2. Geochemical signature of the deformation

The elemental signature of the deformation was clarified by measuring the concentrations of 53 major and trace elements. The concentrations of 10 elements (Be, Bi, Ge, In, K, Na, Mn, Ni, Ti and W) are below detection limits. The concentration versus sample position curves reveal that 24 elements (Al, Cs, Ga, Nb, Rb, Si, Ta, Th, Y, Zr and REE) show strong evidence of variations caused by the development of the studied fault system. The correlation matrix from the normalised principal component analysis of the chemical data-set shows a positive correlation between these 24 elements. This suggests that these 24 elements shared the same behaviour during the deformation.

The Al concentration versus sample position curve (Fig. 6) allows to describe this behaviour. The original chalk from the footwall and the hangingwall shows the same Al signature (1270–1429 ppm). Considering these reference values, it appears that the Al concentration is modified within a 33.5 ± 2 cm wide zone (Fig. 6): 19.6 ± 1 cm in the footwall (samples 1 to 23–25) and 13.9 ± 1 cm in the hangingwall (samples 1 to 14–16). In the footwall as well as in

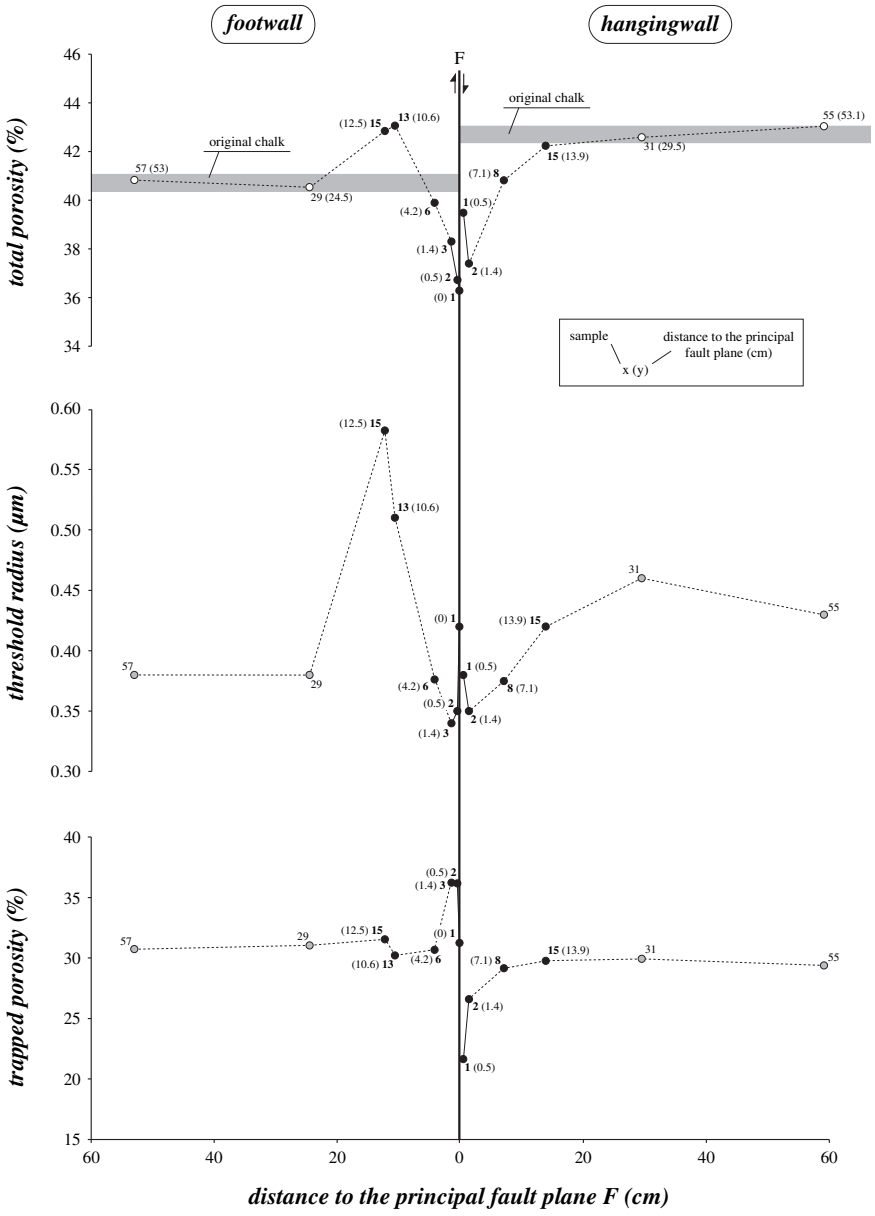

Fig. 4. Evolution of the pore space of chalk through the footwall and the hangingwall of the studied fault system: comparison between the total porosity, the threshold radius and the trapped porosity. In the threshold radius and trapped porosity versus sample position curves, the grey circles indicate the original chalk samples.

the hangingwall, the Al concentration increases within an internal zone (samples 1 to 11–12 and 1 to 3–4 respectively) and decreases within an external zone (samples 12–13 to 15–16 and 4–5 to 14–16 respectively). In the footwall, the Al concentration gradually increases within the internal zone (from samples 11–12 to 2) but the highest value (sample 2: 1746 ppm) is observed at 0.5 cm of the principal fault plane. Within the internal zone of the hangingwall, the highest value (1694 ppm) is also observed near the principal fault plane (between 1.4 and 2.4 cm, samples 2 and 3). An Al enrichment is noticed in the two sides of the subsidiary branch f_1 within a 6.6 ± 1.5 cm wide zone (samples 15–16 to 23–25). On the other hand, no modification in Al concentration is observed in the vicinity of the subsidiary branch f_2.

Unlike REE concentrations, the development of the fault system did not cause modifications in REE pattern. All REE patterns have the same shape (Fig. 7): they show a distinct negative Ce anomaly and a flat baseline reflecting a lack of fractionation between light, middle and heavy REE.

4.3. Mass and volume changes

4.3.1. Identification of immobile elements

In order to quantify the changes in mass and volume caused by the deformation by using the isocon method, immobile elements must be first identified (Grant, 2005). A previous contribution about the Oligocene deformation of the Coniacian chalk in the Paris Basin (Richard, 2008) showed that several major and trace elements (Al, Si and REE particularly) can be considered as immobile elements when the pressure solution-fracturing interactions affect a “white chalk” in an unconfined near-surface meteoric environment. Evidence suggests that Al, Si and REE can be also considered as immobile elements in the present investigation:

- the clay association of the deformed chalk was protected from significant diagenetic effects during and after the deformation because (1) the clay association consists of smectite and illite (Richard et al., 2005), (2) the deformation results from

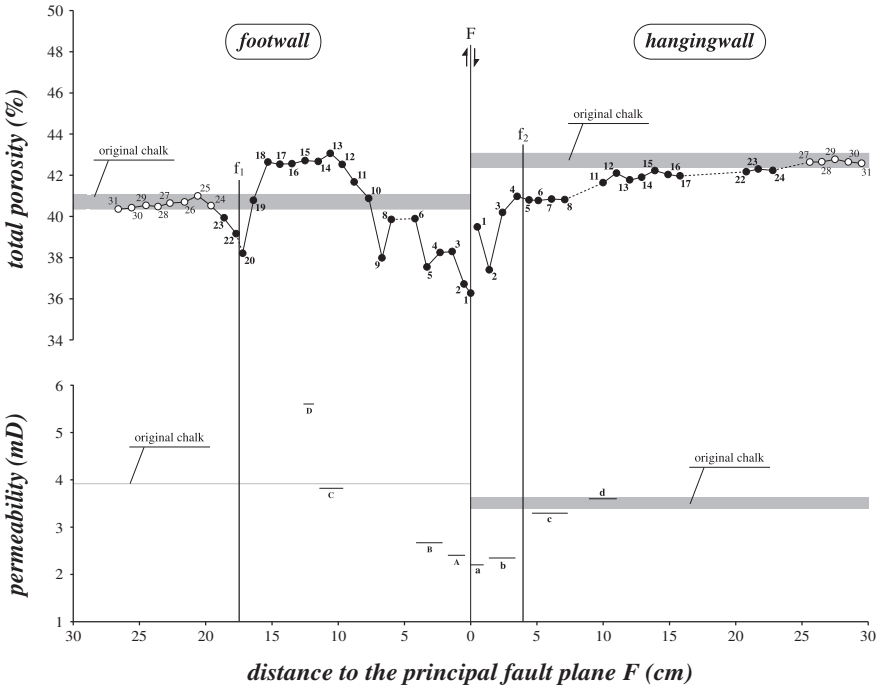

Fig. 5. Comparison of changes in total porosity and permeability of chalk through the footwall and the hangingwall of the studied fault system.

a synsedimentary tectonic activity in a near-surface marine environment (Section 5.1) and (3) the Campanian chalk from the Mons Basin does not show any evidence of burial diagenesis (Richard et al., 2005);

- no evidence of dissolution and/or precipitation of silica are observed in SEM and polarized light microscopy;
- the REE pattern does not show any modification caused by the deformation (Section 4.2).

The correlation matrix from the normalised principal component analysis of the chemical data-set indicates that Al, Cs, Ga, Nb, Rb, Si, Ta, Th, Y, Zr and REE are correlated. This positive correlation reveals that these 24 elements can be considered as immobile elements during the deformation.

4.3.2. Analytical data used

The mass and volume changes (Fig. 8) were quantified by using the Al concentrations because the normalised principal component analysis of immobile element contents indicates that Al has the highest mean correlation coefficient (0.968).

The calculation of mass and volume changes was based on Eqs. (6) and (7) (Section 3.3):

$$V^O/V^A = \left(C_i^A/C_i^O\right) \times \left(\rho^A/\rho^O\right)$$

$$M^O/M^A = \left(\rho^O/\rho^A\right) \times \left(V^O/V^A\right) = C_i^A/C_i^O$$

To use Eqs. (6) and (7), it is necessary to determinate the Al concentrations in the original and altered rocks (C_i^0 and C_i^A

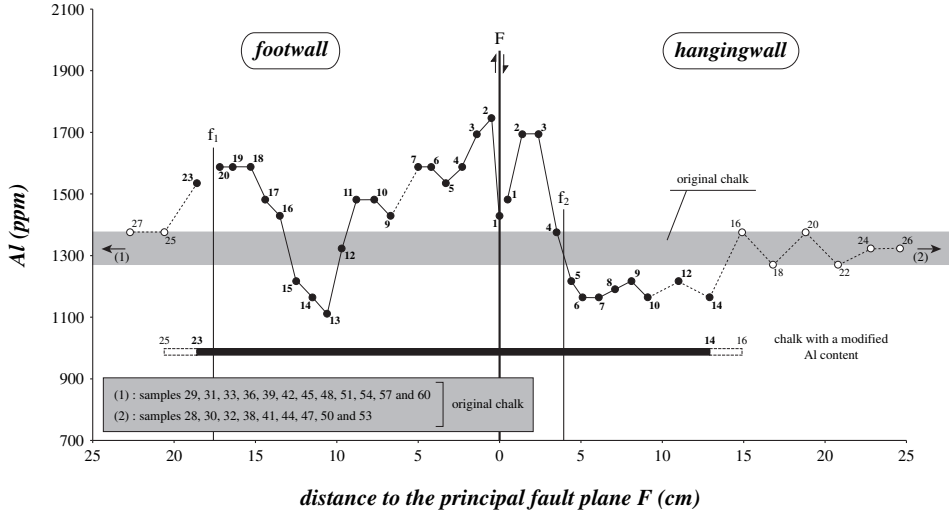

Fig. 6. Evolution of the Al concentration of chalk through the footwall and the hangingwall of the studied fault system.

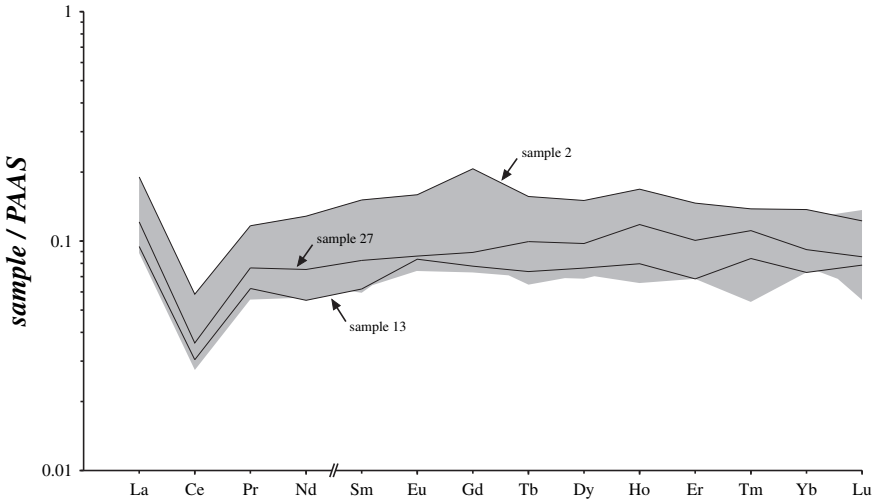

Fig. 7. REE concentration (log scale) versus atomic number. The REE contents are normalised to the Post-Archean Australian Average Shale (PAAS) values proposed by McLennan (1989). The grey area indicates the range of REE concentrations. The black lines represent the REE patterns of samples 27 (original chalk), 2 (increase in REE contents, internal zone) and 13 (decrease in REE contents, external zone) collected in the footwall.

respectively) and the corresponding bulk densities (ρ^O and ρ^A). The original chalk from the footwall and the hangingwall has the same Al signature (C_i^O = 1270 to 1429 ppm, Section 4.2). The bulk density versus sample position curve shows that the original chalk from the footwall and the hangingwall has two different signatures. The footwall and the hangingwall were therefore studied by using different reference values: $\rho^O_{footwall} = 1.594 - 1.645$ and $\rho^O_{hangingwall} = 1.540 - 1.562$.

4.3.3. Quantification and spatial distribution of mass and volume changes

The spatial distribution of mass and volume changes linked to the principal fault plane is similar in the footwall and the hangingwall (Fig. 8): the mass and volume decrease in the internal zones and increase in the external zones.

The mass and volume losses are similar in the footwall and hangingwall internal zones (Fig. 8): the highest mass losses are 23.5% (sample 2) and 21.1% (samples 2 and 3) respectively and the highest volume losses are 28.1% (sample 2) and 27.9% (sample 2) respectively. These highest mass and volume changes are not observed on the principal fault plane but slightly further (Fig. 8). The affected zone is larger in the footwall (9.2 ± 0.5 cm) than in the hangingwall (3.4 ± 0.5 cm).

The mass gains observed in the external zones are close (Fig. 8): the highest mass gains are 20.2% in the footwall (sample 13) and 14.7% in the hangingwall (samples 6, 7 and 14). On the other hand, the volume gains are more different (Fig. 8): the highest volume gains are 25.6% in the footwall (sample 13) and 13.0% in the hangingwall (sample 14). The affected zone is larger in the hangingwall (9.9 ± 1.5 cm) than in the footwall (2.8 ± 1.0 cm).

Mass and volume losses are observed in the vicinity of the subsidiary branch f_1 within 6.6 ± 1.5 cm (samples 15–16 to 23–25) and 5.6 ± 1.5 cm (samples 16–17 to 23–25) wide zones respectively (Fig. 8). The highest mass (15.9%, samples 18, 19 and 20) and volume (18.5%, sample 20) losses are lower than those linked to the principal fault plane (−7.6% and −9.6% respectively). No mass and volume change is related to the subsidiary branch f_2 (Fig. 8).

4.3.4. Comparison between the mass and volume changes and the total porosity modifications

The decreases (and the increases) in total porosity result from mass and volume losses as well as mass and volume gains (Fig. 9). The modifications in total porosity are in fact controlled by the difference in mass and volume changes (mass change < volume change or mass change > volume change, Fig. 9). The samples 15–16 to 24–27 collected in the hangingwall show low decreases in total porosity without any change in mass and volume (Fig. 9).

4.4. Nannofacies modifications

The petrophysical data and the spatial distribution of mass and volume changes allowed to select samples for SEM observations.

4.4.1. Nannofacies of the original chalk

The nannofacies of the original chalk (Fig. 10A) consists of coccospheres (scarse), intact or broken coccoliths and anhedral primary particles (a primary particle is one isolated constituent plate of coccolith). The content of intact coccoliths is important. The constituent plates of coccoliths and the primary particles show smooth faces and their shape is regular. Few secondary particles related to the cementation of primary particles and/or coccolith fragments are observed. The original chalk displays a point-contact fabric.

4.4.2. Nannofacies of the deformed chalk

The SEM observations allowed to study:

- the nannofacies of the deformed chalk showing a mass and volume loss and a total porosity decrease (footwall sample 9 to hangingwall sample 4, Fig. 9): this diagenetic evolution (Fig. 10B) consists of a decrease in amount of coccoliths (the intact coccoliths are scarse) that often display constituent plates with an irregular shape. The primary particles show an anhedral morphology with an irregular shape or a change in morphology (from anhedral to subhedral or euhedral) linked to overgrowths. The content of primary particles decreases but their average size increases. The amount of secondary particles increases. Their morphology is subhedral or euhedral. Dissolution pits are observed on the free faces of particles. The nucleation of new crystals (authigenic particles) is limited except at the rim of pores. All these modifications induced a progressive evolution from a point-contact to a welded fabric with straight or curved sutured contacts. This more dense packing leads to a significant reduction in total porosity. At the SEM scale, the modifications of the chalk fabric are not uniform

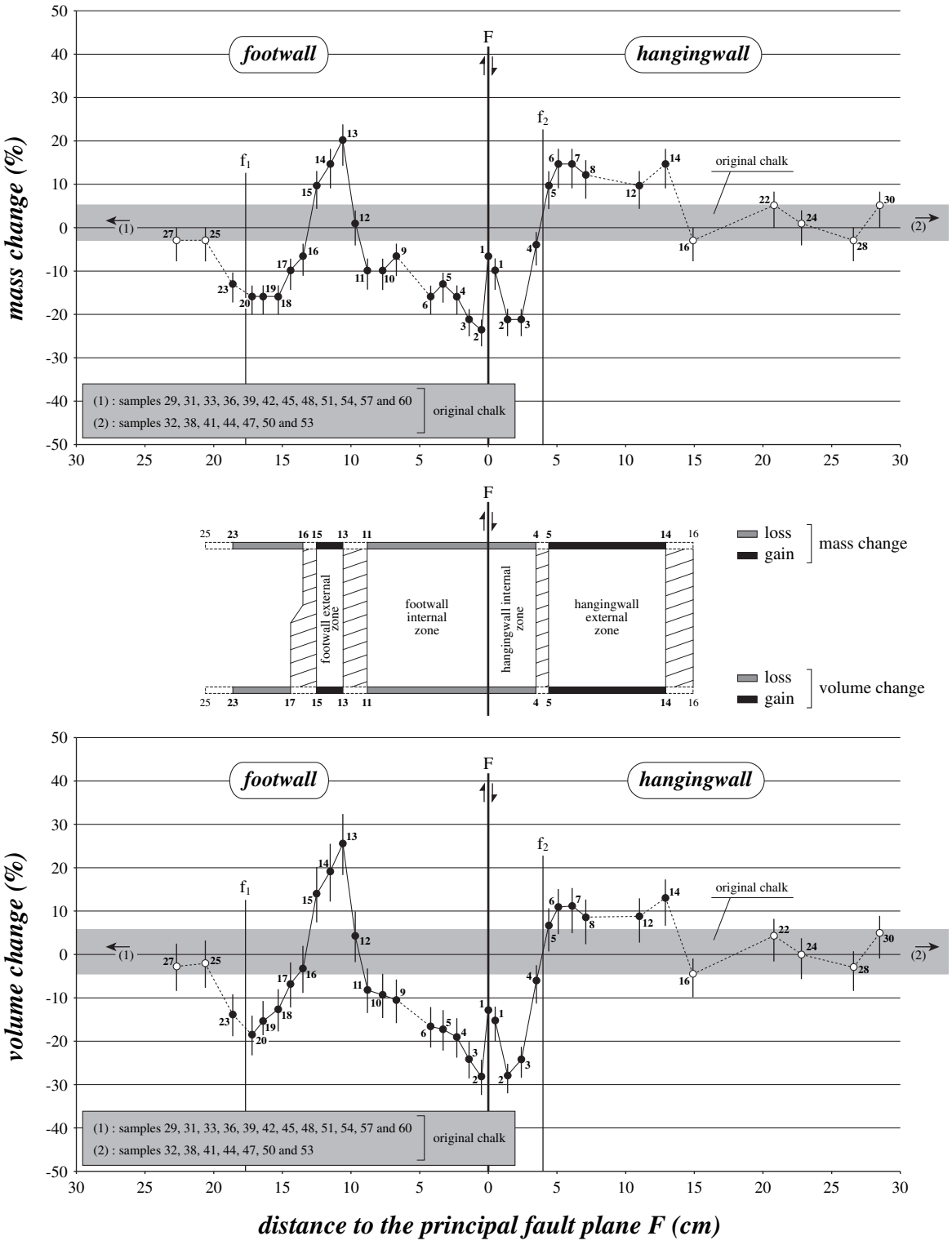

Fig. 8. Quantification and spatial distribution of mass and volume changes resulting from pressure solution-fracturing interactions related to the development of the studied fault system. The circles indicate the mass and volume changes calculated by using the mean values of Al content and bulk density of the original chalk. The vertical lines represent the range of changes in mass and volume calculated by considering the range of Al content and bulk density of the original chalk.

(one sample always shows several fabrics). On the principal fault plane, the main fabric is the coalescent fabric (Fig. 10C).

- the nannofacies of the deformed chalk showing a mass and volume gain and a total porosity increase (footwall samples 13, 14 and 15, Fig. 9): this nannofacies (Fig. 10D) shows an important amount of intact or broken coccoliths and primary particles. The constituent plates of coccoliths and the primary particles are anhedral and regular with smooth faces like in the original chalk. They do not show evidence of dissolution. The diagenetic evolution consists of an increase in content of

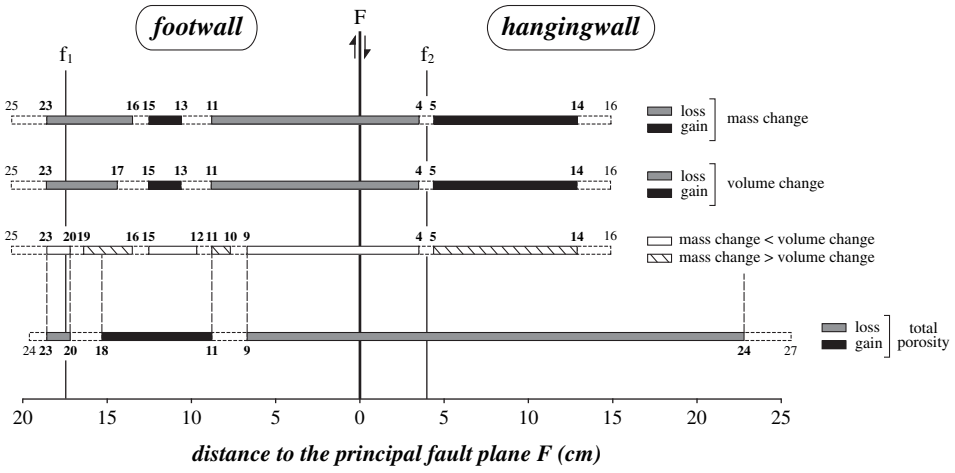

Fig. 9. Comparison between the mass and volume changes and the modifications in total porosity through the footwall and the hangingwall of the studied fault system.

secondary particles and the nucleation of authigenic particles. The morphology of these secondary and authigenic particles is subhedral or euhedral. Their growth induced an increase in average size of particles without fabric change: the fabric is a point-contact fabric like in the original chalk. No decrease in total porosity is observed. These diagenetic modifications appear homogeneous at the SEM scale.

5. Interpretation and discussion

5.1. Diagenetic environment

The fault system studied in the present contribution results from the development of a normal fault related to the Late Campanian NW–SE extension (Section 3.1). Normal faulting linked to

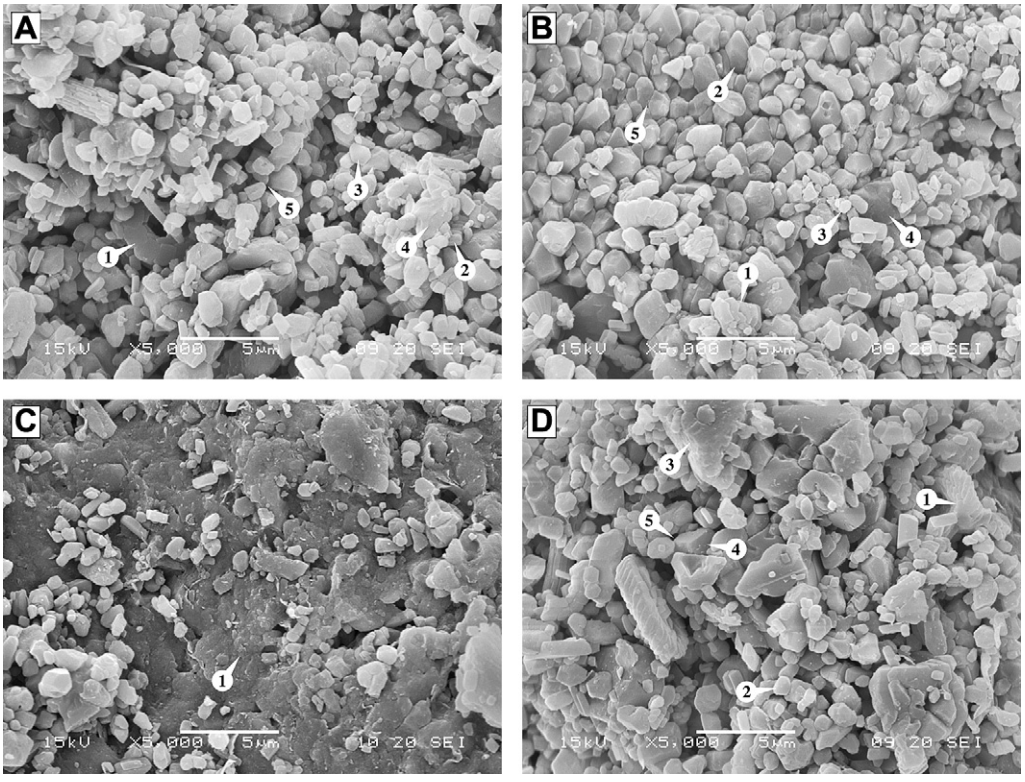

Fig. 10. Evolutions of the nannofacies of the Campanian chalk from the Mons Basin resulting from pressure solution-fracturing interactions linked to the development of the studied fault system. (A) Original chalk (footwall sample 27): [1] intact coccolith showing constituent plates with smooth faces and a regular shape, [2] broken coccolith, [3] primary particle with smooth faces and a regular shape, [4] secondary particle (cementation of primary particles and/or coccolith fragments) and [5] point contacts. (B) Deformed chalk (mass and volume loss with a total porosity decrease, footwall sample 3): [1] broken coccolith showing constituent plates with an irregular shape linked to dissolution on the free faces, [2] primary particle with a euhedral morphology caused by overgrowths, [3] primary particle with an anhedral morphology and an irregular shape resulting from dissolution, [4] euhedral secondary particle and [5] straight sutured contact. (C) Principal fault plane (footwall): [1] coalescent fabric. (D) Deformed chalk (mass and volume gain with a total porosity increase, footwall sample 14): [1] intact coccolith showing constituent plates with a regular morphology and smooth faces like in the original chalk, [2] anhedral primary particle without significant dissolution evidence, [3] secondary particles, [4] euhedral authigenic particle and [5] point contacts.

the Late Campanian NW–SE extension is only observed through the Campanian lithostratigraphic units, never in the Maastrichtian units (Vandycke et al., 1991). Considering the thickness of Campanian lithostratigraphic units from the Harmignies area (Robaszinski and Anciaux, 1996), it is reasonable to consider that the studied fault system developed at depths smaller than 100 m. During the deformation, this near-surface environment was an unconfined phreatic zone with marine interstitial fluids: at the Late Campanian, the Mons Basin was a marine environment and no permeability barrier is observed in the Late Campanian lithostratigraphic succession from the Harmignies area (Richard et al., 2005). The studied deformation therefore results from a synsedimentary tectonic activity in a near-surface marine environment where it affected a weakly cohesive material.

5.2. Diagenetic impact of the principal fault plane

5.2.1. Pore space modifications

5.2.1.1. Reservoir qualities. The development of the fault system modified the total porosity of chalk within a 43.3 ± 1.9 cm wide zone (Section 4.1.1). The spatial distribution of modifications is controlled by the distance to the principal fault plane but the subsidiary branch f_1 also played a significant role (Fig. 3).

In the footwall as well as in the hangingwall, the decrease in total porosity is linked to a decrease in threshold radius (Section 4.1.2). This petrophysical evolution indicates a decrease in pore size and pore-throat size. In the "white chalk", it is reasonable to consider that the trapped porosity is mainly controlled by the ratio $D_{pore}/D_{pore\text{-}throat}$ where D_{pore} is the pore diameter and $D_{pore\text{-}throat}$ the pore-throat diameter. The trapped porosity therefore highlights that the decrease in pore size and pore-throat size occurred without modifications of the ratio $D_{pore}/D_{pore\text{-}throat}$ in the samples showing a low total porosity depletion (footwall sample 6 and hangingwall samples 8 and 15, Fig. 4). In the samples showing a high total porosity depletion (footwall samples 2 and 3 and hangingwall sample 2, Fig. 4), the decrease in pore size and pore-throat size occurred with a modification of the ratio $D_{pore}/D_{pore\text{-}throat}$: in the footwall, the difference between the pore diameter and the pore-throat diameter increases (increase in trapped porosity) whereas, in the hangingwall, it decreases (decrease in trapped porosity).

On the principal fault plane, the chalk shows a specific signature (Sections 4.1.1 and 4.1.2). The comparison between footwall and hangingwall samples 1 and their neighbouring samples (footwall and hangingwall samples 2) reveals that the pore-throat size increases and the difference between the pore diameter and the pore-throat diameter decreases (Fig. 4).

In the footwall, the samples with an increase in total porosity (samples 13 and 15, Fig. 4) show an increase in pore size and pore-throat size without modification of the ratio $D_{pore}/D_{pore\text{-}throat}$.

5.2.1.2. Transport properties. The development of the fault system is at the origin of modifications of the chalk permeability (Section 4.1.3). These modifications are controlled by the distance to the principal fault plane (Fig. 5). The deformation promoted the development of a permeability barrier inside zones adjacent to

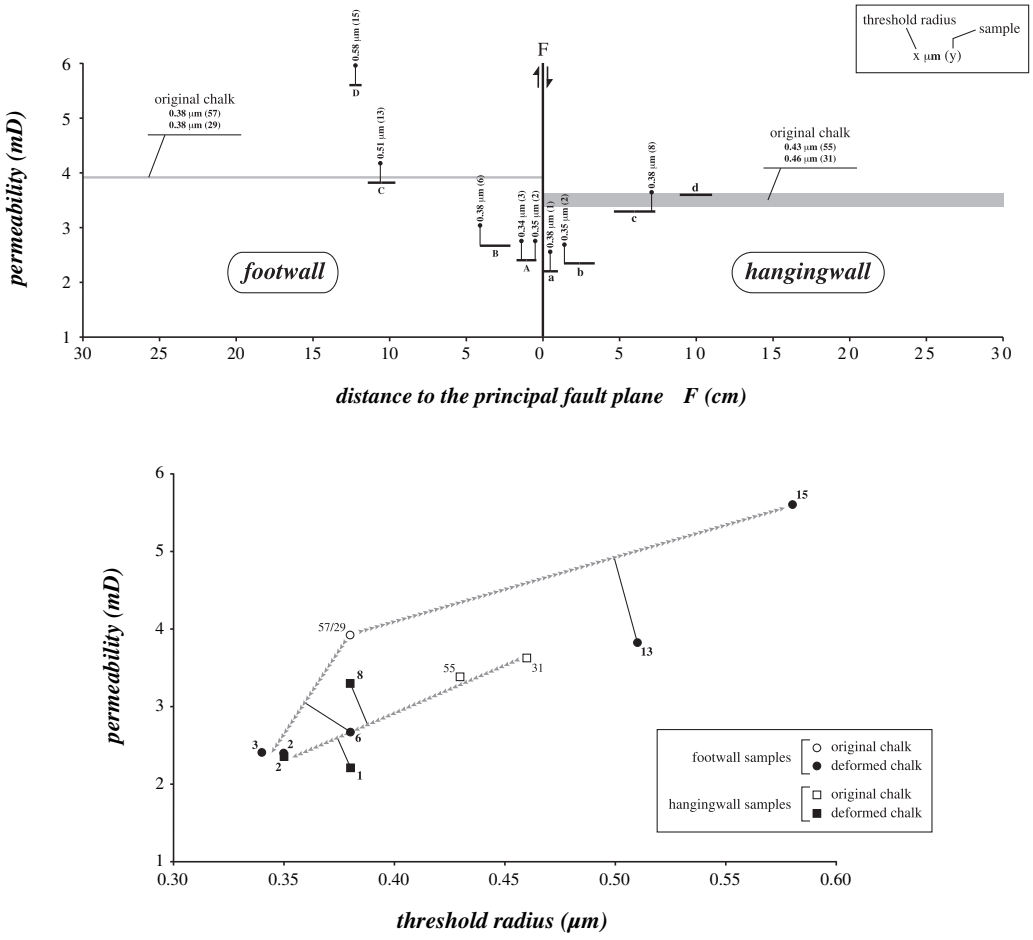

Fig. 11. Comparison between the modifications of threshold radius and the changes in permeability.

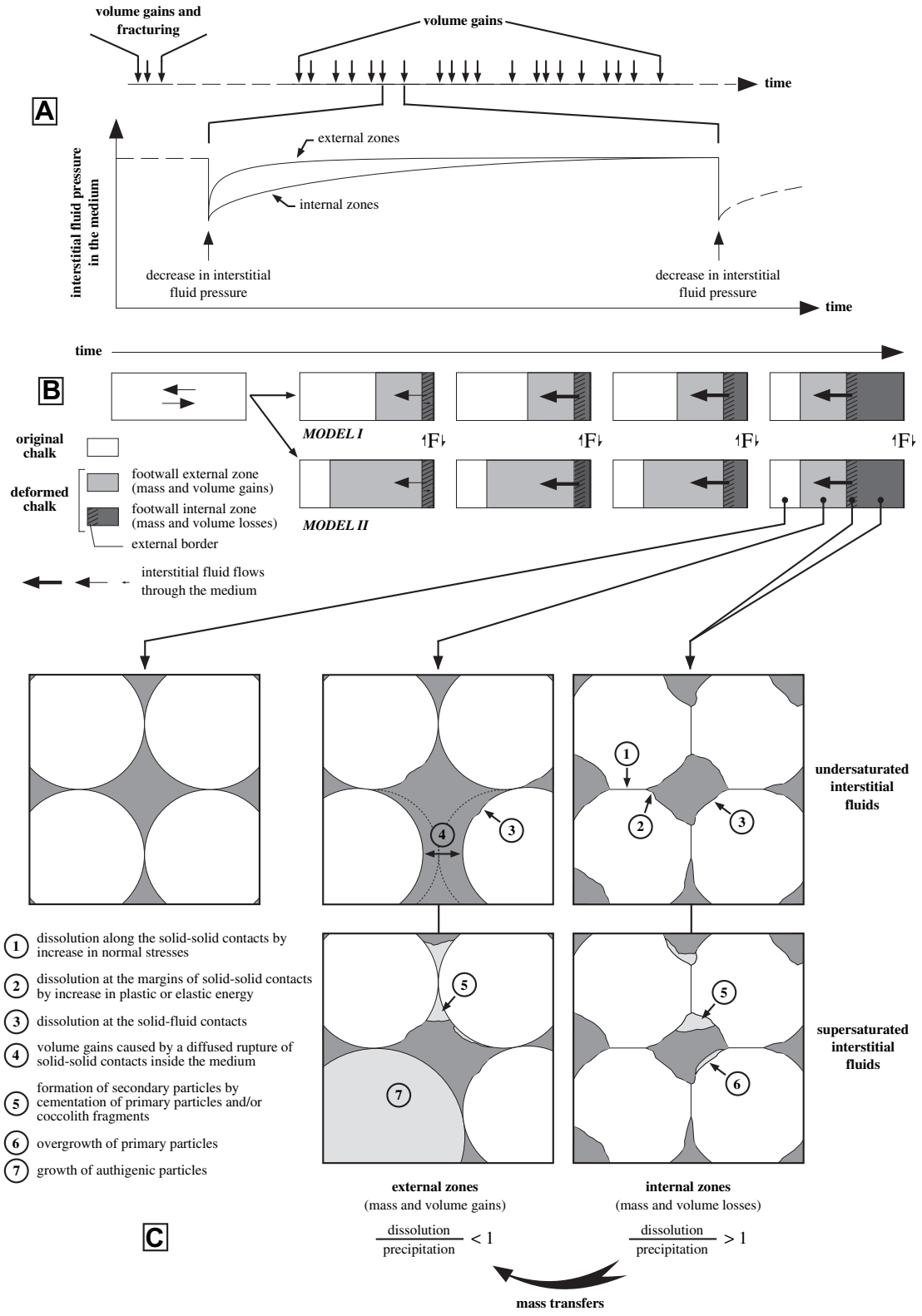

Fig. 12. Conceptual model of the synsedimentary deformation mechanism of the Late Campanian chalk from the Mons Basin. (A) Modifications of the interstitial fluid pressure in the medium. The development of the principal fault plane (with its subsidiary branches) and the volume gains caused by the diffused rupture of grain contacts inside the outermost deformed zones (external zones) trigger repetitive and temporary decreases in interstitial fluid pressure through time. Rapidly, these decreases in interstitial fluid pressure are totally controlled by the volume gains inside the external zones because a permeability barrier develops on the principal fault plane and gradually within adjacent zones (internal zones). The differences in reservoir qualities and transport properties between the chalk of external and internal zones allow a faster return of the interstitial fluid pressure to an initial state in the external zones. The length of time of increases in stress–strain energy is indeed shorter in the external zones than in the internal zones. (B) Evolution of the interstitial fluid flows through the medium and of the spatial distribution of external and internal deformed zones through time (example of the footwall). Each decrease in interstitial fluid pressure is at the origin of a flow of interstitial fluids through chalk towards the active fractures and the external zones where volume gains occur. The development of a permeability barrier on the principal fault plane, and gradually within the internal zones, rapidly restricts the flow of interstitial fluids towards this active fracture.

the principal fault plane: 4 ± 0.6 cm wide zone in the hangingwall and 6.9 ± 2.7 cm wide zone in the footwall (Section 4.1.3). Within the more external deformed zones, significant modifications are only observed in the footwall where the increase in total porosity can be associated with an increase in permeability (sample D, Fig. 5).

Footwall samples 6 and 13 and hangingwall samples 1 and 8 show a poor correlation between the threshold radius and the permeability (Fig. 11). This evidence indicates that the permeability can be controlled by the petrophysical characteristics of narrow bands or planes that represent a small part of the total pore space. In samples 13 (footwall) and 8 (hangingwall), these narrow bands or planes have an original pore space whereas, in samples 6 (footwall) and 1 (hangingwall), they have a pore space more modified than the adjacent material. In samples 6 and 13 (footwall) and 1 (hangingwall), these narrow bands or planes are parallel or sub-parallel to the principal fault plane whereas, in sample 8 (hangingwall), they are perpendicular to the principal fault plane. It therefore appears that the deformation of the pore space is not homogeneous.

5.2.2. Mass and volume changes at the grain scale

The SEM observations allow to clarify, at the grain scale, the diagenetic processes at the origin of mass and volume changes related to the principal fault plane.

Within the internal zones (from footwall samples 11–12 to hangingwall samples 4–5, Fig. 8), the mass losses result from the dissolution of primary particles and constituent plates of coccoliths (the primary particles and the constituent plates of coccoliths often display an irregular shape linked to the development of dissolution pits and their amount decreases). This dissolution took place at the solid–solid contacts (evolution from point contacts to sutured contacts) and solid-fluid contacts (dissolution pits on the free faces). The change in morphology of some primary particles (from anhedral to subhedral or euhedral), the increase in average size of these primary particles and the increase in amount of secondary particles reveal that precipitation took place in the internal zones despite the mass losses but the dissolution/precipitation ratio is above 1. The progressive evolution from a point-contact fabric to a welded fabric (more dense packing) and the change in solid–solid contacts (from point contacts to sutured contacts) indicate that the volume losses inside the internal zones result from a chemical compaction linked to the mass losses.

Within the external zones (from samples 12–13 to 15–16 in the footwall and from 4–5 to 14–16 in the hangingwall, Fig. 8), the mass gains are related to the formation of secondary particles and the growth of authigenic particles that induced a significant increase in average size of particles. The SEM observations indicate that the dissolution in the external zones is restricted: [1] the evidence of dissolution is scarse, [2] the amount of coccoliths and primary particles is high and [3] the primary particles and the constituent plates of coccoliths are anhedral and regular and they show smooth faces like in the original chalk. Two hypotheses can be proposed to explain the volume gains: a localized rupture of grain contacts at the origin of the formation of microscopic fracture planes or a diffused rupture of grain contacts inside the medium. Considering the permeability data and the SEM observations, it is reasonable to consider that the volume gains in the external zones result from a diffused rupture of grain contacts inside the medium:

- no microscopic fracture plane is observed inside the external zones;
- the permeability that ranges between 3.29 mD and 5.60 mD prohibits the presence of a network of interconnected and open microscopic fractures;
- the samples collected in the external zones do not show any permeability depletion related to precipitation of secondary calcite inside microscopic fracture planes parallel or sub-parallel to the principal fault plane;
- the mass gains related to the formation of secondary particles and the growth of authigenic particles and the increase in average size of particles did not induce a change in fabric (the chalk of external zones displays a point-contact fabric like in the original chalk) nor a reduction in total porosity.

5.2.3. Comparison footwall – hangingwall

The evaluation of mass and volume changes related to the principal fault plane (Fig. 8) suggests that the footwall is more affected than the hangingwall:

- the internal zone characterised by mass and volume losses is wider in the footwall (9.2 ± 0.5 cm) than in the hangingwall (3.4 ± 0.5 cm);
- in the external zones, the highest mass and volume gains are observed in the footwall (sample 13).

One observation seems to go against the above conclusion (Fig. 8): the external zone is wider in the hangingwall (9.9 ± 1.5 cm) than in the footwall (2.8 ± 1.0 cm). But it is reasonable to consider that the development of the subsidiary branch f_1 restricted the diagenetic impact of the principal fault plane in the footwall.

The total porosity modifications related to the principal fault plane show that the hangingwall is more affected than the footwall (Fig. 3): the total porosity is modified within a 15.9 ± 0.5 cm wide zone in the footwall (samples 1 to 18–19) and within a 24.2 ± 1.4 cm wide zone in the hangingwall (samples 1 to 24–27). But it is clear that the development of the subsidiary branch f_1 restricted the diagenetic impact of the principal fault plane (Fig. 3).

The presence of subsidiary branches in the studied fault system does not allow to clarify if the diagenetic impact related to the development of the principal fault plane is more important in the footwall than in the hangingwall.

The interstitial fluids, particularly the interstitial fluids of internal zones, mainly migrate towards the external zones where volume gains occur. At present, two conceptual models about the development of internal and external zones through time can be proposed: model I with a simultaneous development of internal and external zones and model II with a successive development of internal and external zones. In the internal zones, the modifications of the fabric (evolution from a point-contact to a welded fabric) and the pore space (decrease in total porosity and permeability) of the medium gradually restrict the diagenetic impact of repetitive interstitial fluid pressure depletions. This negative feedback is probably at the origin of the migration of the external border of internal zones towards more external zones. (C) Diagenetic processes at the origin of mass transfers and volume changes at the grain scale in the internal and external zones. Inside zones adjacent to the principal fault plane (internal zones), and principally along their external border, each decrease in interstitial fluid pressure leads to an increase in stress–strain energy of grains aggregates and an input of undersaturated interstitial fluids. Dissolution of constituent plates of coccoliths and primary particles therefore takes place along the solid–solid contacts by increase in normal stresses (evolution from point contacts to sutured contacts), at the margins of solid–solid contacts by increase in plastic or elastic energy and at the solid-fluid contacts (dissolution pits on the free faces of particles). A chemical compaction at the origin of volume losses occurs in response to these mass losses. The dissolution that takes place inside zones adjacent to the principal fault plane (internal zones) leads to a supersaturation of interstitial fluids with respect to calcite. Precipitation therefore occurs inside the internal zones (overgrowth of primary particles and formation of secondary particles) but it principally takes place within the external zones (formation of secondary particles and growth of authigenic particles) because the length of time of the increase in stress–strain energy is shorter in the external zones than in the internal zones and the supersaturated fluids migrates towards the external zones where the diffused rupture of grain contacts inside the medium promotes volume gains. The mass transfers resulting from pressure solution-fracturing interactions led by the development of the principal fault plane therefore correspond to a mass redistribution from the internal to the external zones.

5.3. Diagenetic impact of subsidiary branches

Although the present study is not focussed on the diagenetic impact of subsidiary branches, it clearly appears that f_1 and f_2 show different behaviours:

- a decrease in mass, volume and total porosity is observed on both sides of f_1 (Figs. 3 and 8). These diagenetic modifications are similar to those linked to the principal fault plane but they are less important (Sections 4.1.1 and 4.3.3);
- no change in mass, volume and total porosity is related to the development of f_2 (Figs. 3 and 8).

Two phenomena can account for these different behaviours: a difference in throw (a lower throw cause a less important deformation) and/or a difference in distance between subsidiary branch and principal fault plane (the diagenetic impact of subsidiary branches increases with the distance to the principal fault plane).

5.4. Conceptual model of the deformation mechanism

A physico-chemical model of the deformation mechanism can be proposed by considering all the data detailed above (Fig. 12). The studied fault system results from a synsedimentary tectonic activity in an unconfined and phreatic near-surface marine environment where it affected a weakly cohesive material (Section 5.1). The development of the principal fault plane (with its subsidiary branches) and the volume gains caused by the diffused rupture of grain contacts in the outermost deformed zones (external zones) trigger repetitive and temporary decreases in interstitial fluid pressure through time (Fig. 12A). Each decrease in interstitial fluid pressure is at the origin of an input of undersaturated fluids with respect to calcite and a flow of interstitial fluids through chalk towards the active fractures and the external zones where volume gains occur. The development of a permeability barrier on the principal fault plane, and gradually within adjacent zones (internal zones), restricts the flow of interstitial fluids towards this active fracture (Fig. 12B). It therefore appears that rapidly:

- the decreases in interstitial fluid pressure are mainly controlled by the volume gains caused by the diffused rupture of grain contacts in the external zones (Fig. 12A);
- the interstitial fluids, particularly the interstitial fluids of internal zones, mainly migrate towards the external zones where volume gains occur (Fig. 12B).

Within zones adjacent to the principal fault plane (internal zones), and principally along their external borders, each decrease in interstitial fluid pressure triggers an increase in stress–strain energy of grains aggregates and an input of undersaturated interstitial fluids with respect to calcite. Dissolution of constituent plates of coccoliths and primary particles therefore takes place (Fig. 12C) along the solid–solid contacts by increase in normal stresses (evolution from point contacts to sutured contacts), at the margins of solid–solid contacts by increase in plastic or elastic energy and at the solid-fluid contacts (dissolution pits on the free faces of particles). A chemical compaction at the origin of volume losses occurs in response to these mass losses (Fig. 12C). The modifications of the fabric (evolution from a point-contact to a welded fabric) and the pore space (decrease in total porosity and permeability) of the medium gradually restrict the diagenetic impact of interstitial fluid pressure depletions. This negative feedback is probably at the origin of the migration of the external borders of internal zones towards more external zones (Fig. 12B).

The dissolution that takes place within the internal zones leads to a supersaturation of interstitial fluids with respect to calcite. Precipitation therefore occurs inside the internal zones (overgrowth of primary particles and formation of secondary particles) but it mainly takes place inside the external zones (formation of secondary particles and growth of authigenic particles) because:

- the length of time of the increase in stress–strain energy is shorter in the external zones than in the internal zones. The reservoir qualities and the transport properties of chalk of external zones allow a faster return of the interstitial fluid pressure to an initial state (Fig. 12A)
- the supersaturated interstitial fluids migrate towards the external zones where the diffused rupture of grain contacts inside the medium promotes volume gains (Fig. 12B and C).

The mass transfers related to the development of the principal fault plane therefore correspond to a mass redistribution from the internal to the external zones (Fig. 12C). At present, two conceptual models about the development of internal and external zones through time can be proposed (Fig. 12B): model I with a simultaneous development of internal and external zones and model II with a successive development of internal and external zones.

6. Conclusions

The present contribution highlights that the pressure solution-fracturing interactions can promote important diagenetic modifications in reservoir qualities, transport properties, elemental signature and nannofacies of weakly cohesive micritic carbonate materials. This diagenetic evolution results from significant mass transfers and volume changes. Within the deformed zones adjacent to the fault planes, the mass losses and the related chemical compaction lead to a decrease in reservoir qualities of the material and the development of a permeability barrier that rapidly restricts the flow of interstitial fluids through medium towards the active fractures. The deformation is therefore rapidly controlled by the volume gains caused by the diffused rupture of grain contacts inside the outermost deformed zones and not by fracturing. Within the outermost deformed zones, the deformation mechanism allows to maintain or to increase the reservoir qualities and the transport properties of the material.

Acknowledgements

We would like to thank Dr. R.E. Holdsworth, Dr. J.P. Gratier and an anonymous reviewer for their extensive and constructive comments that led to substantial improvements of the manuscript. We thank the CBR (Ciments Belges Réunis) company which allowed us to work in the Hainault–Sambre quarry. You are grateful to O. Fabbri for his comments and English proofreading.

References

Angelier, J., Vandycke, S., Bergerat, F., Gaviglio, P., Schroeder, C., Coulon, M., 2006. Can belemnite distribution reveal pressure-solution processes along faults? A case study in chalk of the Mons basin, Belgium. Journal of Structural Geology 28, 64–82.

Carrio-Schaffhauser, E., Gaviglio, P., 1990. Pressure solution and cementation stimulated by faulting in limestones. Journal of Structural Geology 12, 987–994.

Darquennes, A., Vandycke, S., Schroeder, C., 2007. Deformation in faulted white chalk in Belgium. Geologica Belgica 10, 145–147.

Dullien, F.A.L., 1979. Porous Media: Fluid Transport and Pore Structure. Academic Press, New York, pp. 83–85.

Gaviglio, P., Chaye d'Albissin, M., Bergerat, F., Vandycke, S., 1993. Modifications de texture dans la craie au contact de failles normales: un exemple de graben dans le bassin de Mons (Belgique). Bulletin de la Société Géologique de France 4, 565–575.

Gaviglio, P., Adler, P., Thovert, J.F., Vandycke, S., Bergerat, F., Bekri, S., Lestideau, R., 1997. Grain-scale microstructures and physical properties of faulted chalk. Bulletin de la Société Géologique de France 6, 727–739.
Gaviglio, P., Vandycke, S., Schroeder, C., Coulon, M., Bergerat, F., Dubois, C., Pointeau, I., 1999. Matrix strains along normal fault planes in the Campanian white chalk of Belgium: structural consequences. Tectonophysics 309, 41–56.
Gaviglio, P., Bekri, S., Vandycke, S., Adler, P.M., Schroeder, C., Bergerat, F., Darquennes, A., Coulon, M., 2009. Faulting and deformation in chalk. Journal of Structural Geology 31, 194–207.
Grant, J.A., 1986. The isocon diagram – a simple solution to Gresen' equation for metasomatic alteration. Economic Geology 81, 1976–1982.
Grant, J.A., 2005. Isocon analysis: a brief review of the method and applications. Physics and Chemistry of the Earth 30, 997–1004.
Gratier, J.P., Renard, F., Labaume, P., 1999. How pressure solution creep and fracturing processes interact in the upper crust to make it behave in both a brittle and viscous manner. Journal of Structural Geology 21, 1189–1197.
Gresens, R.L., 1967. Composition-volume relationships of metasomatism. Chemical Geology 2, 47–65.
Hellmann, R., Renders, P.J.N., Gratier, J.P., Guiguet, R., 2002a. Experimental pressure solution compaction of chalk in aqueous solutions. Part 1. Deformation behavior and chemistry. In: Hellmann, R., Wood, S.A. (Eds.), Water-rock Interactions, Ore Deposits, and Environmental Geochemistry, vol. 7. The Geochemical Society, Special Publication, pp. 129–152.
Hellmann, R., Gaviglio, P., Renders, P.J.N., Gratier, J.P., Békri, S., Adler, P., 2002b. Experimental Pressure Solution Compaction of Chalk in Aqueous Solutions. Part 2. Deformation Examined by SEM, Porosimetry, Synthetic Permeability and X-ray Computerized Tomography. Water-Rock Interactions, Ore Deposits and Environmental Geochemistry. In: The Geochemical Society, Special Publication, vol. 7 153–178.
Jones, M.E., Bedford, J., Clayton, C., 1984. On natural deformation mechanisms in the chalk. Journal of the Geological Society London 141, 675–683.
McLennan, S.M., 1989. Rare earth elements in sedimentary rocks: influence of provenance and sedimentary processes. In: Lipin, B.R., McKay, G.A. (Eds.), Geochemistry and Mineralogy of Rare Earth Elements, vol. 21. Mineralogical Society of America, pp. 169–200. Reviews in Mineralogy.
Mimran, Y., 1975. Fabric deformation induced in Cretaceous chalks by tectonic stresses. Tectonophysics 26, 309–316.
Mimran, Y., 1977. Chalk deformation and large-scale migration of calcium carbonate. Sedimentology 24, 333–360.
Richard, J., 2008. Mass transfers and volume changes related to pressure solution-fracturing interactions in carbonate rocks: example of the Oligocene deformation of the Coniacian chalk from the Omey area (Paris Basin, France). Journal of Structural Geology 30, 1300–1313.
Richard, J., Coulon, M., Gaviglio, P., 2002. Mass transfer controlled by fracturing in micritic carbonate rocks. Tectonophysics 350, 17–33.
Richard, J., Sizun, J.-P., Machhour, L., 2005. Environmental and diagenetic records from a new reference section for the Boreal realm: the campanian chalk of the Mons basin (Belgium). Sedimentary Geology 178, 99–111.
Robaszinski, F., Anciaux, L., 1996. Les reserves de craie pour ciment blanc sur les propriétés CBR à Harmignies. Report of the Ciment Belges Réunis company.
Schroeder, C., Gaviglio, P., Bergerat, F., Vandycke, S., Coulon, M., 2006. Faults and matrix deformations in chalk: contribution of porosity and sonic wave velocity measurements. Bulletin de la Société Géologique de France 4, 203–213.
Vandycke, S., 2002. Palaeostress records in Cretaceous formations in NW Europe: extensional and strike-slip events in relationships with Cretaceous-tertiary inversion tectonics. Tectonophysics 357, 119–136.
Vandycke, S., Bergerat, F., 1989. Analyse microtectonique des deformations cassantes dans le Bassin de Mons. Reconstitution des paléo-champs de contrainte au Crétacé-Tertiaire. Annales de la Scociété Géologique de Belgique 112, 469–478.
Vandycke, S., Bergerat, F., Dupuis, C., 1988. Paléo-contraintes à la limite Crétacé-Tertiaire dans le Bassin de Mons (Belgique). Implications cinématiques. Relations avec la zone de Cisaillement Nord-Artois. Comptes rendus de l'Académie des Sciences II 307, 303–309.
Vandycke, S., Bergerat, F., Dupuis, C., 1991. Meso-Cenozoic faulting and inferred palaeostresses in the Mons basin, Belgium. Tectonophysics 192, 261–271.